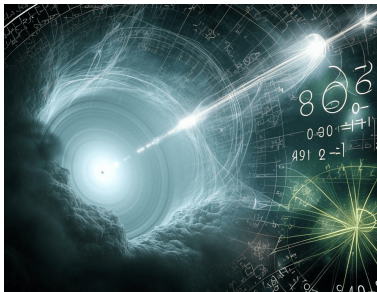


# Searching for Signatures of Internal Gamma-ray Absorption in High-redshift Blazars

A. Dmytriiev<sup>1</sup>, A. Acharyya<sup>2</sup>, M. Böttcher<sup>1</sup>

<sup>1</sup> NWU, Potchefstroom, South Africa, <sup>2</sup> CP3-origins, SDU, Odense, Denmark



High-Energy Astrophysics in Southern Africa (HEASA) 2024 – Wits Rural Facility

# Outline

- 1 Introduction to Blazars
  - Blazars: what can spectra tell us?
  - $\gamma$ - $\gamma$  opacity
- 2 Searching for Opacity Features in High-z Blazars
  - Source selection and data analysis
  - Opacity model
  - Optical data: target photon field
  - Modeling results
  - Implications
- 3 Future work and prospects
- 4 Summary

# Outline

- 1 Introduction to Blazars
  - Blazars: what can spectra tell us?
  - $\gamma$ - $\gamma$  opacity
- 2 Searching for Opacity Features in High-z Blazars
  - Source selection and data analysis
  - Opacity model
  - Optical data: target photon field
  - Modeling results
  - Implications
- 3 Future work and prospects
- 4 Summary

# Blazars: phenomenon and properties

**Blazars** – radio-loud AGN with a jet aligned with the line of sight

- non-thermal emission from radio to  $\gamma$ -rays
- two-bump SED
- highly variable!
  - **Flares:** flux  $\nearrow$  by a factor  $\sim 10$  over short time-scales minutes – weeks
  - **High states:**  $t_{\text{var}} \sim$  weeks – years

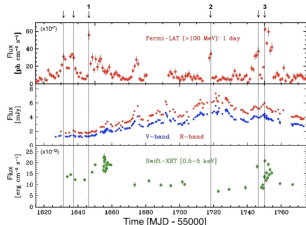


Figure: Multi-band light curves of 3C 279 variability.

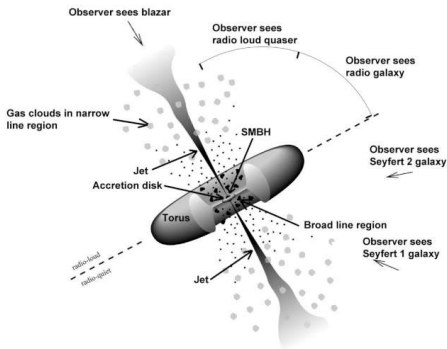


Figure: Unified view of an AGN (credit: Urry & Padovani (1995))

## Spectral information: measurement of MWL SEDs

## ● Emitting particle spectra

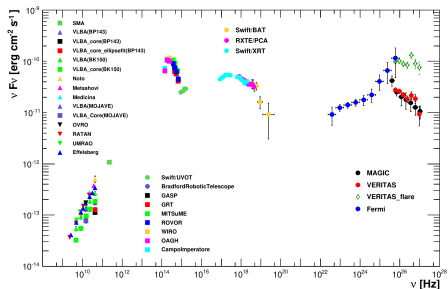
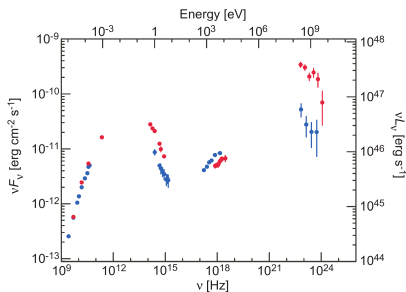


Figure: Left: nearly-simultaneous spectral measurements combined across different spectral ranges for two activity states of 3C 279 (credit: Abdo et al. (2010)). Right: multi-band spectral data of Mrk 501 taken during an observational campaign in 2009 (credit: Abdo et al. (2011)).

## Spectral information: measurement of MWL SEDs

- Emitting particle spectra
- Physical conditions in the emitting zone

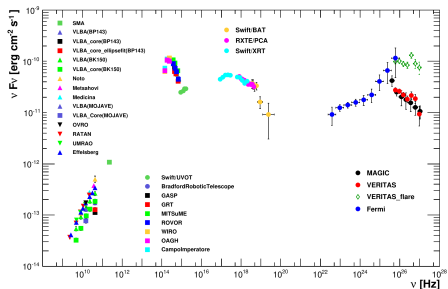
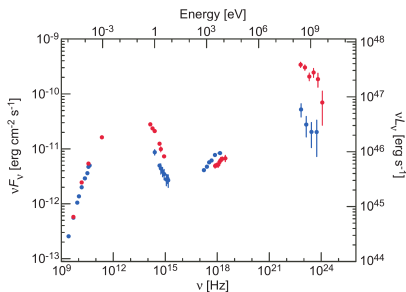


Figure: Left: nearly-simultaneous spectral measurements combined across different spectral ranges for two activity states of 3C 279 (credit: Abdo et al. (2010)). Right: multi-band spectral data of Mrk 501 taken during an observational campaign in 2009 (credit: Abdo et al. (2011)).

# Spectral information: measurement of MWL SEDs

- Emitting particle spectra
- Physical conditions in the emitting zone
- MWL emission origin

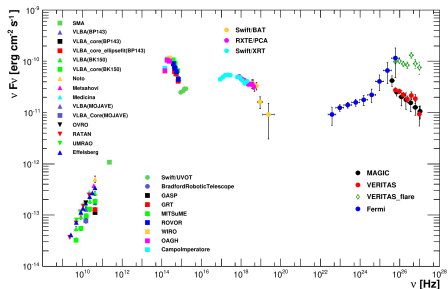
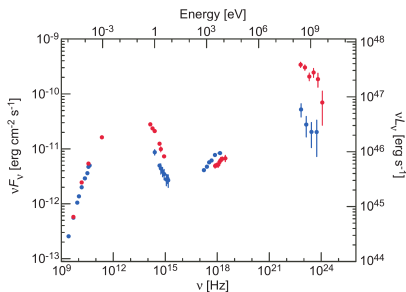


Figure: Left: nearly-simultaneous spectral measurements combined across different spectral ranges for two activity states of 3C 279 (credit: Abdo et al. (2010)). Right: multi-band spectral data of Mrk 501 taken during an observational campaign in 2009 (credit: Abdo et al. (2011)).

## Spectral information: measurement of MWL SEDs

- Emitting particle spectra
- Physical conditions in the emitting zone
- MWL emission origin
- Contributions of different emission components

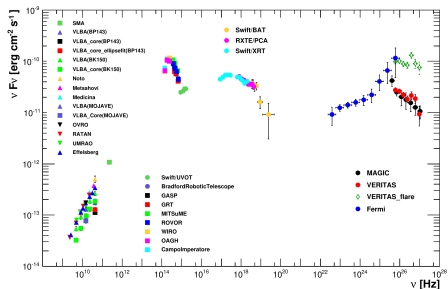
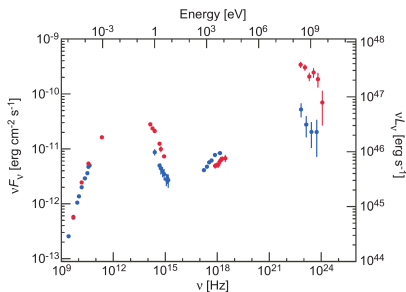


Figure: Left: nearly-simultaneous spectral measurements combined across different spectral ranges for two activity states of 3C 279 (credit: Abdo et al. (2010)). Right: multi-band spectral data of Mrk 501 taken during an observational campaign in 2009 (credit: Abdo et al. (2011)).



# Spectral information: measurement of MWL SEDs

- Emitting particle spectra
- Physical conditions in the emitting zone
- MWL emission origin
- Contributions of different emission components
- Physical processes / acceleration mechanisms

Fermi-I? Fermi-II? magnetic reconnection?

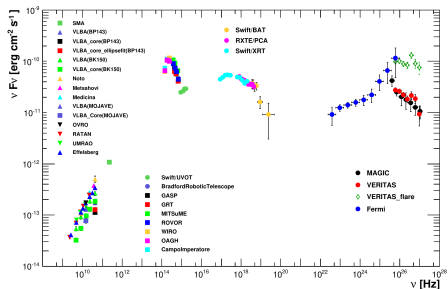
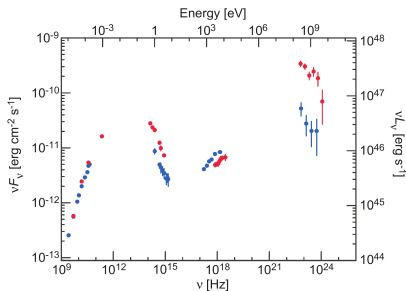
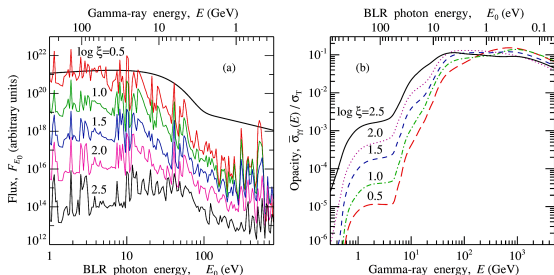


Figure: Left: nearly-simultaneous spectral measurements combined across different spectral ranges for two activity states of 3C 279 (credit: Abdo et al. (2010)). Right: multi-band spectral data of Mrk 501 taken during an observational campaign in 2009 (credit: Abdo et al. (2011)).

## Different target radiation fields

Depending on location of  $\gamma$ -ray emitting zone in the jet,  $\gamma$ -rays are exposed to different photon fields:

- **Accretion disk** (UV,  $r \lesssim 0.01$  pc)
- **Broad line region** (optical-UV,  $r \sim 0.01 - 0.1$  pc)
- **Dusty torus** (infrared,  $r \gtrsim 0.1$  pc)



**Figure:** Left: typical spectrum of BLR. Right:  $\gamma$ - $\gamma$  absorption cross-section (relative to  $\sigma_T$ ) on BLR photon field for different energies of  $\gamma$ -rays.  
Credit: Poutanen & Stern (2010)

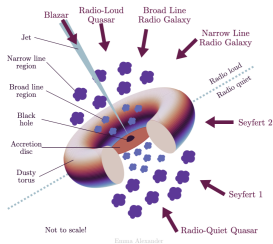


**Figure:** Scheme illustrating different AGN components. Credit: Emma Alexander

$\gamma - \gamma$  absorption: theory

$$\gamma + \gamma \rightarrow e^- + e^+$$

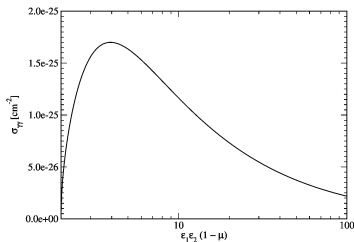
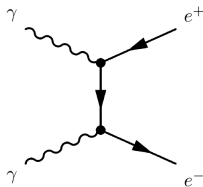
Threshold of pair production:  $\epsilon_1 \epsilon_2 \geq 2(1 - \mu)^{-1}$ ,  $\mu = \cos \theta$

Cross-section (angle-dependent):

$$\sigma_{\gamma\gamma}(\epsilon_1, \epsilon_2, \mu) = \frac{3}{16} \sigma_T (1 - y^2) \left( [3 - y^4] \times \ln \left[ \frac{1+y}{1-y} \right] - 2y[2 - y^2] \right)$$

$$\text{with } y = \sqrt{1 - 2/(\epsilon_1 \epsilon_2 [1 - \mu])}$$

Peak in cross-section at  $x = \epsilon_1 \epsilon_2 (1 - \mu) = 4$  ( $\epsilon = 2\epsilon_{\text{thr}}$ ), with  $\sigma_{\gamma\gamma}^{\text{peak}} \approx 0.25 \sigma_T$



## Absorption features due to different target radiation fields

Target photon fields with different spectra induce different absorption features in observed  $\gamma$ -ray spectra

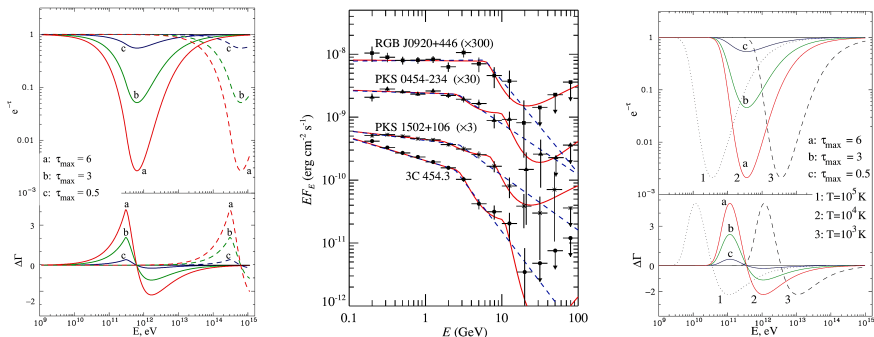


**Figure:** Opacity features induced by power-law seed photon field (left), BLR field (center) and blackbody (right).  
Credit: Poutanen & Stern (2010) and Aharonian et al. (2008)

# Outline

- 1 Introduction to Blazars
  - Blazars: what can spectra tell us?
  - $\gamma$ - $\gamma$  opacity
- 2 Searching for Opacity Features in High-z Blazars
  - Source selection and data analysis
  - Opacity model
  - Optical data: target photon field
  - Modeling results
  - Implications
- 3 Future work and prospects
- 4 Summary

## Motivation of our study

- For **high-z** sources, the opacity features move to **lower energies** in the  $\gamma$ -ray spectra

## Motivation of our study

- For **high-z** sources, the opacity features move to **lower energies** in the  $\gamma$ -ray spectra
- Interaction with **Ly  $\alpha$**  photons (10.2 eV):  
 $E_\gamma \approx 25 \text{ GeV}/(1 + z)$

## Motivation of our study

- For **high-z** sources, the opacity features move to **lower energies** in the  $\gamma$ -ray spectra
- Interaction with **Ly  $\alpha$**  photons (10.2 eV):  
 $E_\gamma \approx 25 \text{ GeV} / (1 + z)$
- For  $z = (3 - 4)$ :  
absorption starts from **5 – 6 GeV !**  
→ best *Fermi*-LAT sensitivity !



## Motivation of our study

- For **high-z** sources, the opacity features move to **lower energies** in the  $\gamma$ -ray spectra
- Interaction with **Ly  $\alpha$**  photons (10.2 eV):  
 $E_\gamma \approx 25 \text{ GeV}/(1 + z)$
- For  $z = (3 - 4)$ :  
absorption starts from **5 – 6 GeV !**  
→ best *Fermi*-LAT sensitivity !
- **Strong** optical/ $\gamma$ -ray signal → **high accretion disk luminosity**  
→ **stronger opacity**

## Motivation of our study

- For **high-z** sources, the opacity features move to **lower energies** in the  $\gamma$ -ray spectra
- Interaction with **Ly  $\alpha$**  photons (10.2 eV):  
 $E_\gamma \approx 25 \text{ GeV}/(1 + z)$
- For  $z = (3 - 4)$ :  
absorption starts from **5 – 6 GeV !**  
→ best *Fermi*-LAT sensitivity !
- **Strong** optical/ $\gamma$ -ray signal → **high accretion disk luminosity**  
→ **stronger opacity**
- **What can we learn?**
  - (1) The location of  $\gamma$ -ray production site in the jet
  - (2) Distribution of target photon fields within the source
  - (3) Emission scenarios
  - (4) Constraints on the opacity: how  $\gamma$ -rays avoid absorption?

## Source selection

We select **9**  $\gamma$ -ray detected FSRQs with  $z > 3$  (Paliya et al. (2020))

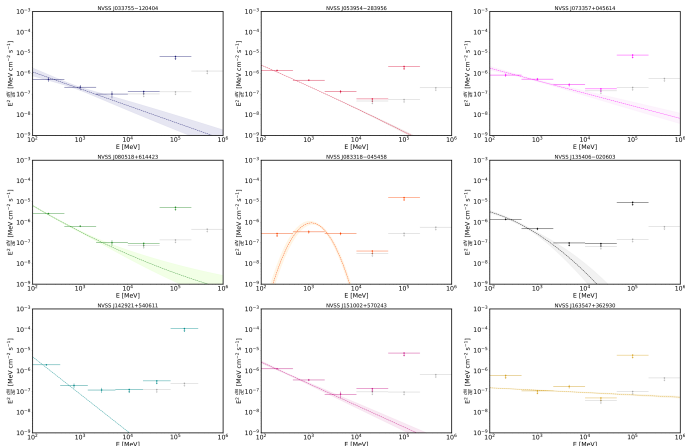
Name	R.A. (deg)	Decl. (deg)	Redshift	$R_{\text{mag}}$	$F_{\text{radio}}$ (mJy)
$\gamma$ -Ray-detected blazars					
NVSS J033755–120404	54.48104	–12.06793	3.442	20.19	475.3
NVSS J053954–283956	84.97617	–28.66554	3.104	18.97	862.2
NVSS J073357+045614	113.48941	4.93736	3.01	18.76	218.8
NVSS J080518+614423	121.32575	61.73992	3.033	19.81	828.2
NVSS J083318–045458	128.32704	–4.9165	3.5	18.68	356.5
NVSS J135406–020603	208.52873	–2.10089	3.716	19.64	733.4
NVSS J142921+540611	217.34116	54.10309	3.03	19.84	1028.3
NVSS J151002+570243	227.51216	57.04538	4.313	19.89	202.0
NVSS J163547+362930	248.94681	36.49164	3.615	20.55	151.8

# Fermi-LAT data analysis

## Analysis: A. Acharyya

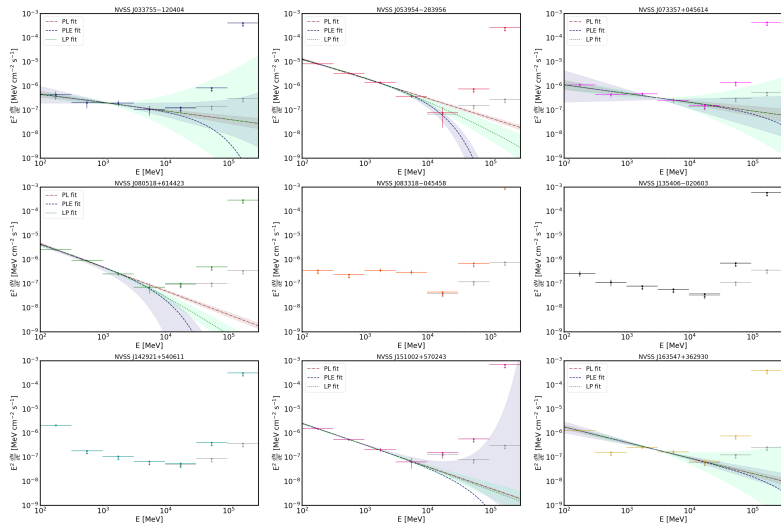
- Energy range: 0.1 GeV – 1 TeV
- **1.5 bins per decade of energy** (6 bins / 4 decades)
- 15 years of data

- Standard selection cuts
- Spectral model:  
4FGL catalog shape  
(power law / logparabola)



## Fermi-LAT data analysis

- 2 bins per decade of energy (used for the modeling)



## Model for $\gamma\text{-}\gamma$ absorption in the BLR

We use the model and code by [Böttcher & Els \(2016\)](#)

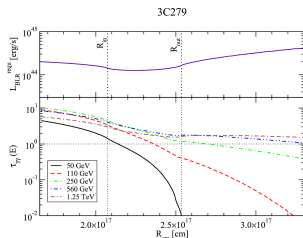
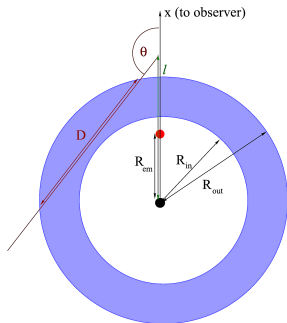
- Full **angle-dependent**  $\gamma\text{-}\gamma$  absorption cross-section
- **BLR geometry**: a shell with inner and outer radius  $R_1$  and  $R_2$ . Assume  $u_{\text{BLR}} = \text{const}$  everywhere
- Computes **optical depth**  $\tau$  as a function of  $\gamma$ -ray energy  $E_\gamma$  and distance of the emitting zone from the central engine  $R_{\text{ez}}$

$$u_{\text{BLR}} = \int_0^\infty d\epsilon \int_0^\infty dr 2\pi \int_{-1}^1 r^2 d\mu \frac{j_\epsilon(r)}{4\pi r^2 c} =$$

$$= \frac{1}{2c} \int_0^\infty d\epsilon j_\epsilon^0 \int_{-1}^1 d\mu D(\mu)$$

$$\tau_{\gamma-\gamma}(\epsilon_\gamma, d) = \frac{1}{2c} \int_{R_{\text{ez}}}^\infty dl \int_{-1}^1 d\mu \int_0^\infty d\epsilon \frac{j_\epsilon^0 D(\mu)}{\epsilon m_e c^2} \times$$

$$\times (1 - \mu_i) \sigma_{\gamma-\gamma}(\epsilon_\gamma, \epsilon, \mu_i)$$



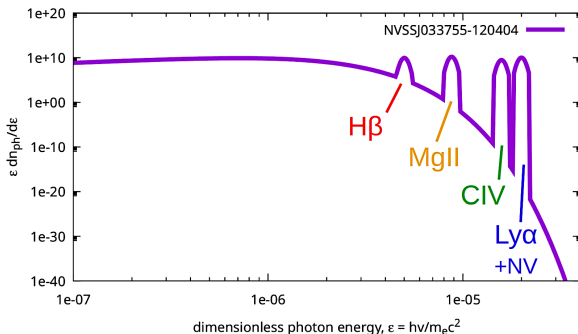
## Target radiation field: $u_{\nu,\text{rad}}(\nu)$

We use a template for BLR spectrum with a **blackbody continuum** ( $T = 1500$  K) and a **set of 4 emission lines** as measured in real optical data. We assume that the total BLR luminosity (sum of 4 lines + continuum) is (always) 10% of  $L_D$

$$u_{\text{line}} = \frac{L_{\text{line}}}{4\pi R_{\text{BLR}}^2 c}$$

$$u_{\text{cont}} = u_{\text{BLR,tot}} - \frac{\sum L_{\text{line}}}{4\pi R_{\text{BLR}}^2 c}$$

$$u_{\text{BLR,tot}} = \frac{0.1 L_D}{4\pi R_{\text{BLR}}^2 c}$$



## Luminosity of the accretion disk

We assume that the **BLR** dominates the target radiation field, with the BLR covering fraction 10%

$$u_{\text{BLR,tot}} = \frac{0.1 L_{\text{D}}}{4\pi R_{\text{BLR}}^2 c}$$

$$R_{\text{BLR}} \approx 0.1 L_{\text{D},46}^{1/2} \text{ pc}$$

e.g. Hayashida et al. (2012)

We adopt  $L_{\text{D}}$  from [Paliya et al. \(2020\)](#) – estimates based on broadband SED modeling

Source #	Name (NVSS)	$\log_{10}(L_{\text{D}} \text{ erg s}^{-1})$
1	NVSS J033755-120404	46.36
2	NVSS J053954-283956	46.70
3	NVSS J073357+045614	46.60
4	NVSS J080518+614423	46.34
5	NVSS J083318-045458	47.15
6	NVSS J135406-020603	46.78
7	NVSS J142921+540611	46.26
8	NVSS J151002+570243	46.63
9	NVSS J163547+362930	46.30



## Luminosity of optical BLR emission lines

- We use available luminosities of the most prominent optical emission lines

## Luminosity of optical BLR emission lines

- We use available luminosities of the most prominent optical emission lines
- **L $\alpha$**  (1216 Å) + **N V** (1240 Å), **C IV** (1549 Å), **Mg II** (2798 Å) and **H $\beta$**  (4861 Å)

## Luminosity of optical BLR emission lines

- We use available luminosities of the most prominent optical emission lines
- **L $\gamma\alpha$**  (1216 Å) + **N V** (1240 Å), **C IV** (1549 Å), **Mg II** (2798 Å) and **H $\beta$**  (4861 Å)
- Need to know  $L_{L\gamma\alpha}$  (+N V) very accurately  
→ induces opacity features at lowest  $\gamma$ -ray energies

## Luminosity of optical BLR emission lines

- We use available luminosities of the most prominent optical emission lines
- **L $\gamma\alpha$**  (1216 Å) + **N V** (1240 Å), **C IV** (1549 Å), **Mg II** (2798 Å) and **H $\beta$**  (4861 Å)
- Need to know  $L_{L\gamma\alpha}$  (+N V) very accurately  
→ induces opacity features at lowest  $\gamma$ -ray energies
- We adopt  $L_{MgII}$  and  $L_{H\beta}$  from an IR study by [Burke et al. \(2024\)](#)

## Luminosity of optical BLR emission lines

- We use available luminosities of the most prominent optical emission lines
- **L $\gamma$**  (1216 Å) + **N V** (1240 Å), **C IV** (1549 Å), **Mg II** (2798 Å) and **H $\beta$**  (4861 Å)
- Need to know  $L_{L\gamma\alpha}$  (+N V) very accurately  
→ induces opacity features at lowest  $\gamma$ -ray energies
- We adopt  $L_{\text{MgII}}$  and  $L_{\text{H}\beta}$  from an IR study by [Burke et al. \(2024\)](#)
- We adopt  $L_{\text{CIV}}$  from [Paliya et al. \(2021\)](#) (except source #3)

## Luminosity of optical BLR emission lines

- We use available luminosities of the most prominent optical emission lines
- **$\text{Ly}\alpha$**  (1216 Å) +  **$\text{N V}$**  (1240 Å),  **$\text{C IV}$**  (1549 Å),  **$\text{Mg II}$**  (2798 Å) and  **$\text{H}\beta$**  (4861 Å)
- Need to know  $L_{\text{Ly}\alpha}$  (+N V) very accurately  
→ induces opacity features at lowest  $\gamma$ -ray energies
- We adopt  $L_{\text{MgII}}$  and  $L_{\text{H}\beta}$  from an IR study by [Burke et al. \(2024\)](#)
- We adopt  $L_{\text{CIV}}$  from [Paliya et al. \(2021\)](#) (except source #3)
- **For  $L_{\text{Ly}\alpha}$**  (includes N V):

## Luminosity of optical BLR emission lines

- We use available luminosities of the most prominent optical emission lines
- **L $\gamma\alpha$**  (1216 Å) + **N V** (1240 Å), **C IV** (1549 Å), **Mg II** (2798 Å) and **H $\beta$**  (4861 Å)
- Need to know  $L_{L\gamma\alpha}$  (+N V) very accurately  
→ induces opacity features at lowest  $\gamma$ -ray energies
- We adopt  $L_{\text{MgII}}$  and  $L_{\text{H}\beta}$  from an IR study by [Burke et al. \(2024\)](#)
- We adopt  $L_{\text{CIV}}$  from [Paliya et al. \(2021\)](#) (except source #3)
- **For  $L_{L\gamma\alpha}$**  (includes N V):
  - source #1, 2: **old measurements** from [Osmer et al. \(1994\)](#) only

## Luminosity of optical BLR emission lines

- We use available luminosities of the most prominent optical emission lines
- **L $\gamma$  $\alpha$**  (1216 Å) + **N V** (1240 Å), **C IV** (1549 Å), **Mg II** (2798 Å) and **H $\beta$**  (4861 Å)
- Need to know  $L_{L\gamma\alpha}$  (+N V) very accurately  
→ induces opacity features at lowest  $\gamma$ -ray energies
- We adopt  $L_{\text{MgII}}$  and  $L_{\text{H}\beta}$  from an IR study by [Burke et al. \(2024\)](#)
- We adopt  $L_{\text{CIV}}$  from [Paliya et al. \(2021\)](#) (except source #3)
- **For  $L_{L\gamma\alpha}$**  (includes N V):
  - source #1, 2: **old measurements** from [Osmer et al. \(1994\)](#) only
  - source #3: **prediction derived** using scaling as by average ratios of [Francis et al. \(1991\)](#) (as well as for  $L_{\text{CIV}}$ )



## Luminosity of optical BLR emission lines

- We use available luminosities of the most prominent optical emission lines
- **L $\gamma\alpha$**  (1216 Å) + **N V** (1240 Å), **C IV** (1549 Å), **Mg II** (2798 Å) and **H $\beta$**  (4861 Å)
- Need to know  $L_{L\gamma\alpha}$  (+N V) very accurately  
→ induces opacity features at lowest  $\gamma$ -ray energies
- We adopt  $L_{MgII}$  and  $L_{H\beta}$  from an IR study by [Burke et al. \(2024\)](#)
- We adopt  $L_{CIV}$  from [Paliya et al. \(2021\)](#) (except source #3)
- **For  $L_{L\gamma\alpha}$**  (includes N V):
  - source #1, 2: **old measurements** from [Osmer et al. \(1994\)](#) only
  - source #3: **prediction derived** using scaling as by average ratios of [Francis et al. \(1991\)](#) (as well as for  $L_{CIV}$ )
  - source #4, 5: **no information at all** (and the measured line ratios are *inconsistent* with Francis et al.)

## Luminosity of optical BLR emission lines

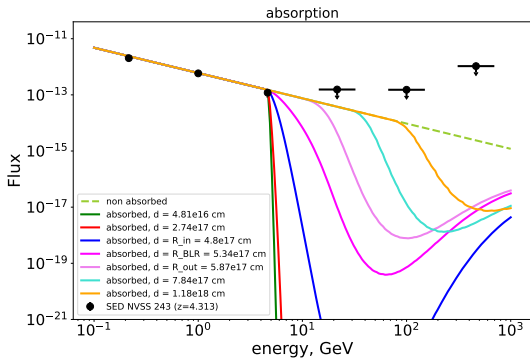
- We use available luminosities of the most prominent optical emission lines
- **Ly $\alpha$**  (1216 Å) + **N V** (1240 Å), **C IV** (1549 Å), **Mg II** (2798 Å) and **H $\beta$**  (4861 Å)
- Need to know  $L_{\text{Ly}\alpha}$  (+N V) very accurately  
→ induces opacity features at lowest  $\gamma$ -ray energies
- We adopt  $L_{\text{MgII}}$  and  $L_{\text{H}\beta}$  from an IR study by [Burke et al. \(2024\)](#)
- We adopt  $L_{\text{CIV}}$  from [Paliya et al. \(2021\)](#) (except source #3)
- **For  $L_{\text{Ly}\alpha}$**  (includes N V):
  - source #1, 2: **old measurements** from [Osmer et al. \(1994\)](#) only
  - source #3: **prediction derived** using scaling as by average ratios of [Francis et al. \(1991\)](#) (as well as for  $L_{\text{CIV}}$ )
  - source #4, 5: **no information at all** (and the measured line ratios are *inconsistent* with Francis et al.)
  - source #6, 7, 8, 9: **accurate measurement** through **SDSS DR18**

## Luminosity of optical BLR emission lines

Source #	Name (NVSS)	z	$\log_{10}(L_{Ly\alpha+NV})$	$\log_{10}(L_{CIV})$	$\log_{10}(L_{MgII})$	$\log_{10}(L_{H\beta})$
1	J033755-120404	3.442	44.8941	$44.268 \pm 0.193$	$44.73 \pm 0.09$	$44.24 \pm 0.05$
2	J053954-283956	3.104	44.7335	$45.091 \pm 0.091$	$44.38 \pm 0.04$	$43.21 \pm 0.09$
3	J073357+045614	3.01	$44.613 \pm 0.063$	$44.412 \pm 0.063$	$44.09 \pm 0.02$	$44.01 \pm 0.06$
4	J080518+614423	3.033	x	$44.743 \pm 0.095$	$44.39 \pm 0.03$	$43.79 \pm 0.06$
5	J083318-045458	3.5	x	$45.220 \pm 0.111$	$44.63 \pm 0.01$	$44.47 \pm 0.01$
6	J135406-020603	3.716	$45.092 \pm 0.027$	$44.552 \pm 0.038$	$44.39 \pm 0.06$	$43.95 \pm 0.09$
7	J142921+540611	3.03	$44.36 \pm 0.04$	$44.241 \pm 0.018$	$44.07 \pm 0.09$	$43.79 \pm 0.11$
8	J151002+570243	4.313	$45.245 \pm 0.019$	$44.857 \pm 0.059$	$44.84 \pm 0.09$	x
9	J163547+362930	3.615	$44.8 \pm 0.22$	$44.305 \pm 0.023$	$44.42 \pm 0.02$	$43.75 \pm 0.04$

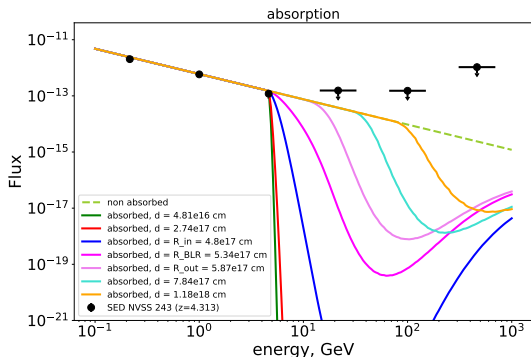
## Approach

- We **fit** each spectrum with a **power law** or **logparabola** (4FGL catalog shape)



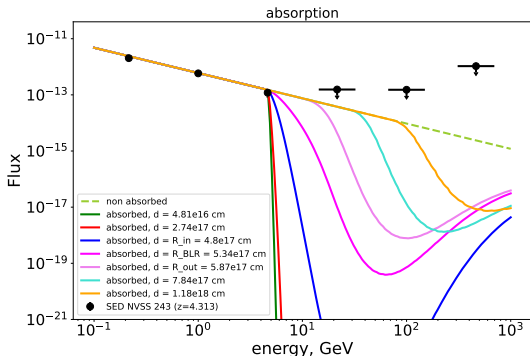
## Approach

- We **fit** each spectrum with a **power law** or **logparabola** (4FGL catalog shape)
- We  $\gamma$ - $\gamma$  **absorb** each model using the opacity code (with the relevant  $L_D$ ), while varying the location of the  $\gamma$ -ray production region



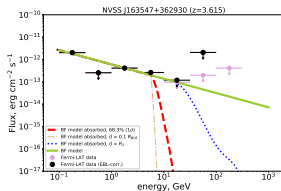
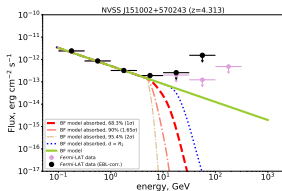
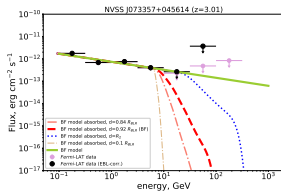
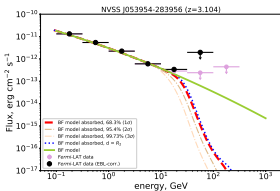
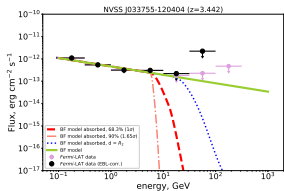
## Approach

- We **fit** each spectrum with a **power law** or **logparabola** (4FGL catalog shape)
- We  $\gamma$ - $\gamma$  **absorb** each model using the opacity code (with the relevant  $L_D$ ), while varying the location of the  $\gamma$ -ray production region
- Folded model (average over bins):  
 $\chi^2 \leq \chi_{\min}^2 + 1$  indicates allowed locations in the jet ( $1\sigma$ )



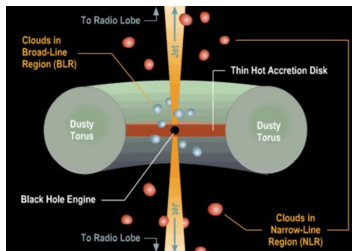
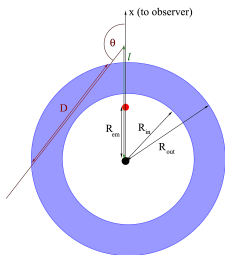
## Fit results

- 3/9 sources do not have enough statistics
- Of remaining 6 sources, 5 have  $\text{Ly}\alpha$  information available
- **Lower limit** of distance from SMBH (only) for 4/9 sources
- Spectrum of Source #3 is **consistent with opacity model**



Constraints on the  $\gamma$ -ray production zone location

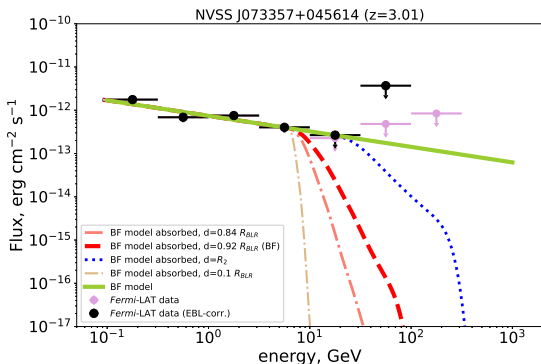
Source #	Name (NVSS)	$R_{\text{BLR}}$ (cm)	$R_{\text{ez}}/R_{\text{BLR}}$ ( $1\sigma$ )	... ( $1.65\sigma$ )	$\chi^2_{\nu}$ (non-abs)
1	J033755-120404	$4.67 \times 10^{17}$	$\geq 0.92$	$\geq 0.48$	2.43/2
2	J053954-283956	$6.9 \times 10^{17}$	$\geq 1.08$	$\geq 1.06$	3.84/2
3	J073357+045614	$6.16 \times 10^{17}$	$= 0.92$	$=$	5.13/2
4	J080518+614423	—	—	—	—
5	J083318-045458	—	—	—	—
6	J135406-020603	—	—	—	—
7	J142921+540611	—	—	—	—
8	J151002+570243	$6.37 \times 10^{17}$	$\geq 1.01$	$\geq 0.92$	2.57/2
9	J163547+362930	$4.36 \times 10^{17}$	$\geq 0.84$	NA	0.76/1





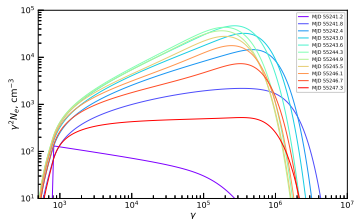
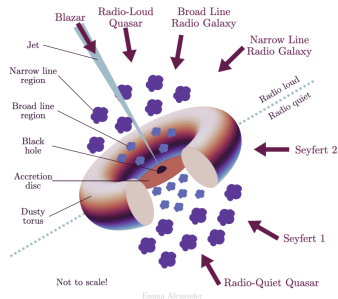
## Particular case: Source #3

- Spectrum of Source #3 is **consistent with opacity model**
- An improved  $\chi^2$  ( $\Delta\chi^2 < 0$ ) is achieved for the **absorbed model** in the range  $R_{\text{ez}}/R_{\text{BLR}} \geq 0.84$
- The best fit is achieved for  $R_{\text{ez}}/R_{\text{BLR}} = 0.92 \rightarrow$  emitting zone WITHIN BLR



## Discussion of results

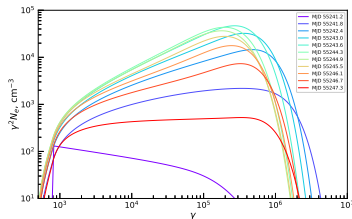
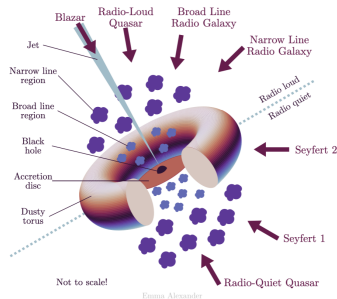
- **The observed cutoff in the  $\gamma$ -ray spectra cannot be distinguished from e.g. cutoff in the particle spectrum**  $\rightarrow$  mostly lower limits on the emitting zone location



## Discussion of results

- **The observed cutoff in the  $\gamma$ -ray spectra cannot be distinguished from e.g. cutoff in the particle spectrum**  $\rightarrow$  mostly lower limits on the emitting zone location
- Very particular location – shocked region in the jet consistently in the vicinity of BLR shell

The emitting zone **cannot be too far** from BLR as well  $\rightarrow$  production of  $\gamma$ -rays via IC

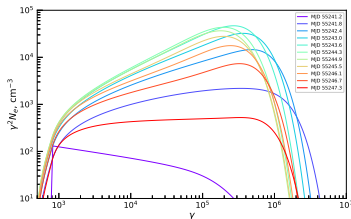
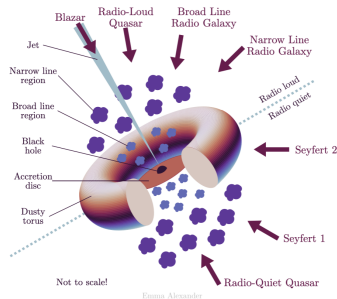


## Discussion of results

- **The observed cutoff in the  $\gamma$ -ray spectra cannot be distinguished from e.g. cutoff in the particle spectrum**  $\rightarrow$  mostly lower limits on the emitting zone location
- Very particular location – shocked region in the jet consistently in the vicinity of BLR shell

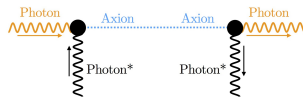
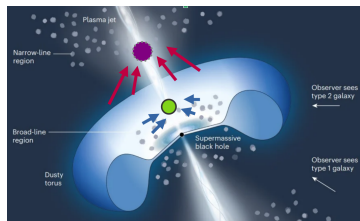
The emitting zone **cannot be too far** from BLR as well  $\rightarrow$  production of  $\gamma$ -rays via IC

- **Source #2 (NVSS J053954-283956)** – tighter constraints can be derived (emitting zone close to inner BLR radius)



## Discussion of results

- **Second emitting zone?**
  - full physical modeling required
  - correlation between different bands
- Hadronic models
  - $p\text{-}\gamma$  process – internal opacity
- Exotic physics, e.g. **photon-axion coupling in magnetic field ?**



# Outline

- 1 Introduction to Blazars
  - Blazars: what can spectra tell us?
  - $\gamma$ - $\gamma$  opacity
- 2 Searching for Opacity Features in High-z Blazars
  - Source selection and data analysis
  - Opacity model
  - Optical data: target photon field
  - Modeling results
  - Implications
- 3 Future work and prospects
- 4 Summary

# Constraining the EBL

- The best-fit  $\chi^2$  for the **EBL-deabsorbed** intrinsic spectrum for different EBL models (Saldana-Lopez 2021; Finke 2022; Franceschini 2018; ...)
  - limited statistics of the data
  - full physical modeling is preferred
- **Statistical approach:** spectral index as a function of redshift  $z$ 
  - limited selection of sources

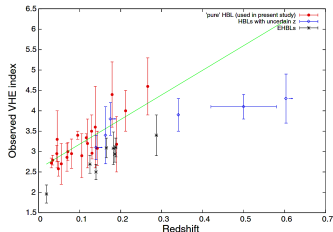
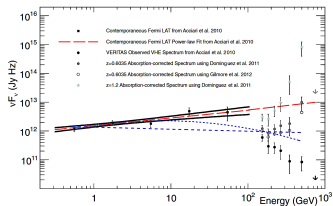
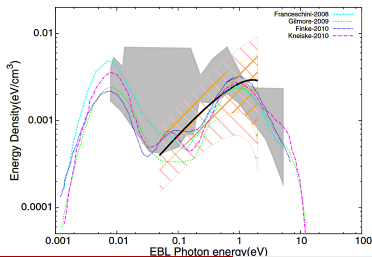


Figure: (Top): example of de-absorption of an observed  $\gamma$ -ray spectrum using different EBL models (Furniss et al. 2013). Bottom: distribution of observed VHE spectral index of a selection of HBLs as a function of redshift (Sinha et al. 2014)

## Studying internal absorption in other blazars

- **Intermediate redshift blazars ( $z=1-2$ ):**  
an optimal balance between the  $\gamma$ -ray statistics and the opacity feature downshift

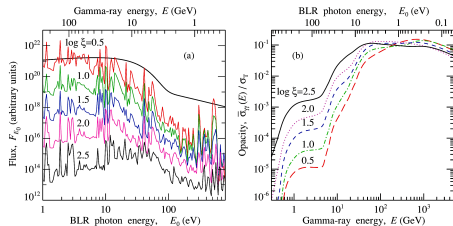


Figure: Left: typical spectrum of BLR. Right:  $\gamma$ - $\gamma$  absorption cross-section (relative to  $\sigma_T$ ) on BLR photon field for different energies of  $\gamma$ -rays.

Credit: Poutanen & Stern (2010)

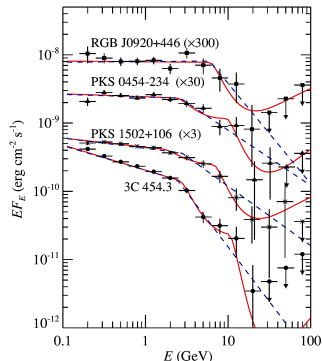


Figure: Opacity features induced by the BLR field (Poutanen & Stern (2010))



## Beyond leptonic models: hadronic scenario

$$\pi^\pm \rightarrow \mu^\pm + \nu_\mu (\bar{\nu}_\mu)$$

$$\mu^\pm \rightarrow e^\pm + \bar{\nu}_\mu (\nu_\mu) + \nu_e (\bar{\nu}_e)$$

### TXS 0506+056

- IceCube  $\sim 290$  TeV  $\nu$  (2017)  
+ GeV (*Fermi*-LAT) and VHE (MAGIC) flare
- $\nu$ -flare (2014 – 2015): no  $\gamma$ -ray activity

Assuming **photo-hadron** (rather than  $p-p$ ):

$$E'_\nu \approx 0.05 E'_p, \quad s \approx E'_\gamma E'_p \approx E_{\Delta^+}^2$$

- **Target field: X-ray** (Böttcher et al. (2022))
  - Synchrotron-supported cascade is ruled out (Reimer et al. (2019))
- ⇒ Target photons originate outside the jet?
- ! GeV  $\gamma$ -rays **absorbed** on the target field
- **Strong  $\nu$  sources: WEAK at GeV  $\gamma$ -ray !**

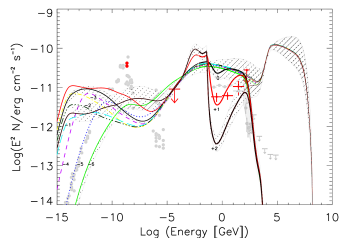
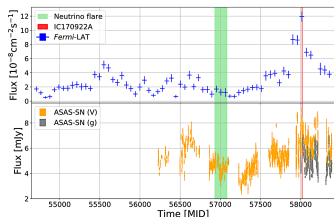


**Figure:** (Top) *Fermi*-LAT and optical LC of TXS 0506+056. Green – neutrino flare in 2014 – 2015. (Bottom) Simulations of synchrotron-supported cascades to generate the observed neutrino flare flux (credit: Reimer et al. (2019))

## Prospects with CTA

The next generation IACT instrument.  
Operational by 202?

**Large Size Telescope (LST)** particularly helpful thanks to the low-energy threshold and sensitivity

- Sensitivity ↗ by a factor of  $\sim 10$
  - Northern and Southern site (La Palma and Chile)
  - Energy range:  $\sim 30 \text{ GeV} - \sim 300 \text{ TeV}$
  - Substantially better angular, spectral and timing resolution
- **Much tighter constraints on  $\gamma$ - $\gamma$  opacity,  $\gamma$ -ray production site location and EBL**

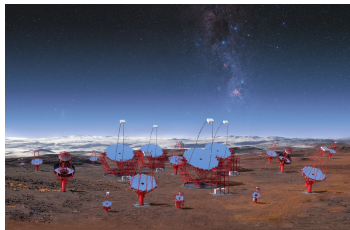


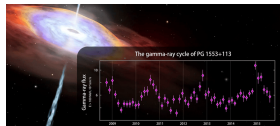
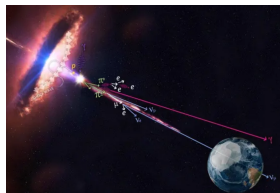
Figure: Top: CGI rendering of the CTA array view; Bottom: LST in La Palma (credit: ESO/CTA)

# Outline

- 1 Introduction to Blazars
  - Blazars: what can spectra tell us?
  - $\gamma$ - $\gamma$  opacity
- 2 Searching for Opacity Features in High-z Blazars
  - Source selection and data analysis
  - Opacity model
  - Optical data: target photon field
  - Modeling results
  - Implications
- 3 Future work and prospects
- 4 Summary

# Summary

- Exploring high-redshift blazars allows to search for  $\gamma$ - $\gamma$  opacity signatures at lower energies
- We established **constraints on the location of the  $\gamma$ -ray production region** in the jet for 5 blazars with redshifts  $z = 3 - 4.3$
- One needs to understand why the  $\gamma$ -ray production (shocked region in the jet) takes place mostly close to the **BLR outer boundary**
- One of the sources displays a possible  **$\gamma - \gamma$  opacity feature** at energy  $\sim 8$  GeV. **Emitting zone located within the BLR close to the INNER boundary**
- Full modeling required – leptonic, hadronic, multi-zone models
- Promising prospects with CTA



⇒ ApJ paper in preparation, to be submitted (hopefully) within this month

# Thank you!

